Two-dimensional to bulk crossover of the WSe2 electronic band structure

Patrick Le Fèvre, Raphaël Salazar, Matthieu Jamet, François Bertran, Chiara Bigi, Abdelkarim Ourghi, Céline Vergnaud, Aki Pulkkinen, Jan Minar, Thomas Jaouen, et al.

Two-dimensional to bulk crossover of the WSe_2 electronic band structure

Raphaël Salazar,[†,‡] Matthieu Jamet,[¶] Céline Vergnaud,[¶] Aki Pulkkinen,[‡] François Bertran,[†] Chiara Bigi,[†] Ján Minár,[‡] Abdelkarim Ouerghi,[§] Thomas Jaouen,[∥] Julien Rault,[†] and Patrick Le Fèvre[*,†,∥]

†*Synchrotron SOLEIL, L'Orme des Merisiers, Départementale 128, F-91190 Saint-Aubin, France*

‡*New Technologies Research Centre, University of West Bohemia, 30614 Pilsen, Czech Republic*

¶*Univ. Grenoble Alpes, CEA, CNRS, Grenoble INP, IRIG-SPINTEC, 38000 Grenoble, France*

§*Université Paris-Saclay, CNRS, Centre de Nanosciences et de Nanotechnologies, 91120, Palaiseau, Paris, France*

∥*Univ Rennes, CNRS, IPR - UMR 6251, F-35000 Rennes, France*

⊥*ABB Switzerland Ltd, Baden Dättwil, Switzerland*

E-mail: patrick.lefevre@univ-rennes.fr

Abstract

Transition Metal Dichalcogenides (TMD) are layered materials obtained by stacking two-dimensional sheets weakly bonded by van der Waals interactions. In bulk TMD, band dispersions are observed in the direction normal to the sheet plane (z-direction) due to the hybridization of out-of-plane orbitals but no k_z-dispersion is expected at the single-layer limit. Using angle-resolved photoemission spectroscopy, we

precisely address the two-dimensional to three-dimensional crossover of the electronic band structure of epitaxial WSe_2 thin films. Increasing number of discrete electronic states appears in given k_z-ranges while increasing the number of layers. The continuous bulk dispersion is nearly retrieved for 6-sheet films. These results are reproduced by calculations going from a relatively simple tight-binding model to a sophisticated KKR-Green's function calculation. This two-dimensional system is hence used as a benchmark to compare different theoretical approaches.

Ever since the discovery of graphene[1,2], research on two-dimensional (2D) materials is ongoing a tremendous effort. Along with this trend, transition metal dichalcogenides (TMD) are extremely promising for possible technological applications. Their general formula is MX_2, where M is a transition element and X is a chalcogene. Those two elements form a MX_2 basic layer, where M atoms are sandwiched between two covalently-bonded planes of chalcogenes. The three-dimensional (3D)-solid is obtained by stacking these X-M-X sheets, only weakly bonded by van der Waals interactions[3], conferring to TMD a very pronounced 2D-character. Nowadays, research pushes towards increasingly elaborated structures taking advantage of the 2D nature of these materials: twisted TMD layers[4], hybrid TMD structures (e.g., $MoSe_2/WSe_2$, WS_2/WSe_2)[5–7] or alloyed TMD systems[8]. In the ideal case, these structures are studied by the means of Angle-Resolved PhotoEmission Spectroscopy (ARPES), a technique which allows for direct measurement of the band structure. Its surface sensitivity makes it particularly well-suited to probe 2D-compounds. For bulk TMD-crystals, despite the expected strong 2D-nature of these materials, a significant band dispersion can be observed perpendicular to the MX_2-sheets[9–11]. As a matter of fact, both the M-d_{z^2} and the X-p_z orbitals (the z-axis being perpendicular to the MX_2-sheets) point out from the MX_2-planes and can hybridize to give rise to this perpendicular dispersion. It can be successfully modeled either using Density Functional Theory (DFT)[10] or a tight-binding approach[11]. Nevertheless, DFT-band structure calculations are often made assuming the 2D character of TMD and obtain results on a mesh with only one k_z point. For instance, from calculations

presented in reference 12, one could hastily conclude that, at low thicknesses, each new layer in the stacking generates an additional band at Γ. Figure 1 shows dispersions measured on a 2-layer WSe_2 sample in directions parallel to $\Gamma - K$ for various photon energies, *i.e.* various position along the $\Gamma - A$ direction. We do observe the expected two bands at 31 and 51 eV-photon energies, but not at 21 and 42 eV. That means that even for ultimately thin samples, k_z-effects can be expected, which is more surprising. Previous work on single and bi-layer MoS_2 already hinted at those conclusions without proposing a complete explanation[13]. These primary observations urge towards a better understanding of the k_z-dependency even for thin samples.

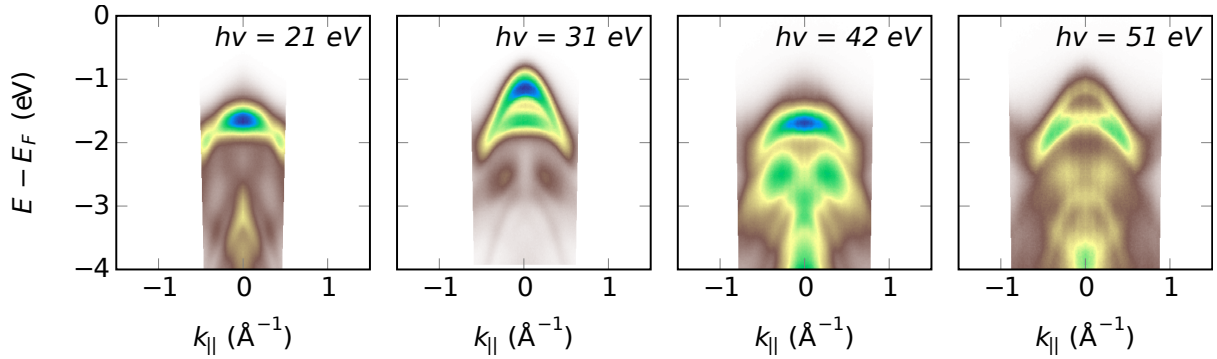

Figure 1: ARPES on 2-layer WSe_2 giving the band-dispersion in directions parallel to $\Gamma - K$ at various photon energies (21, 31, 42 and 51 eV, from left to right). Depending on the photon energy, one or two bands are visible at Γ between -2 eV binding energy and the Fermi level. Spectra have been symmetrized with respect to Γ.

We propose here to study the transition from the 2D-electronic structure of an ultimately thin TMD to a 3D-bulk crystal. We focused on WSe_2, whose electronic structure has already been extensively scrutinized[10–12]. The perpendicular dispersion of the band structure is measured by ARPES for sample thicknesses of 2, 3 and N (=6–7) layers. The 2- and N-layer samples were grown by molecular beam epitaxy (MBE) on graphene/SiC (Gr-SiC). To complete the experiment, a 3-layer sample of WSe_2 was grown on Mica and then wet-transferred onto a Gr-SiC substrate[14,15]. More details about the samples are given in the Supporting Information.

The ARPES measurements were performed at room temperature on the CASSIOPEE

beamline of the SOLEIL synchrotron radiation facility. The samples were first aligned with the Γ-K direction of WSe_2 reciprocal lattice along the slit of the analyzer. We call $k_{\|}$ the component of the wave vector parallel to this direction. A ($k_{\|}$, E_B) image can then be measured at once thanks to the 2D-detector of the electron analyzer. Here, E_B is the electron binding energy and is measured with respect to the Fermi level E_F. k_z was changed by scanning the photon energy from 20 to 90 eV (and 1 eV-step), which amounts to span a k_z-range from roughly 2.5 to 5 $Å^{-1}$. Details on the experimental geometry, on the measurement strategy and on the determination of E_F are given in the Supporting Information.

Figure 2 shows a series of ARPES-images recorded on the N-layer sample showing the dispersion along $k_{\|}$ for chosen photons energies between 20 and 90 eV. It clearly evidences large variations of the band structure along $\Gamma - A$ (see Figure 3(a)). The vertical black line is at $k_{\|}$=0.

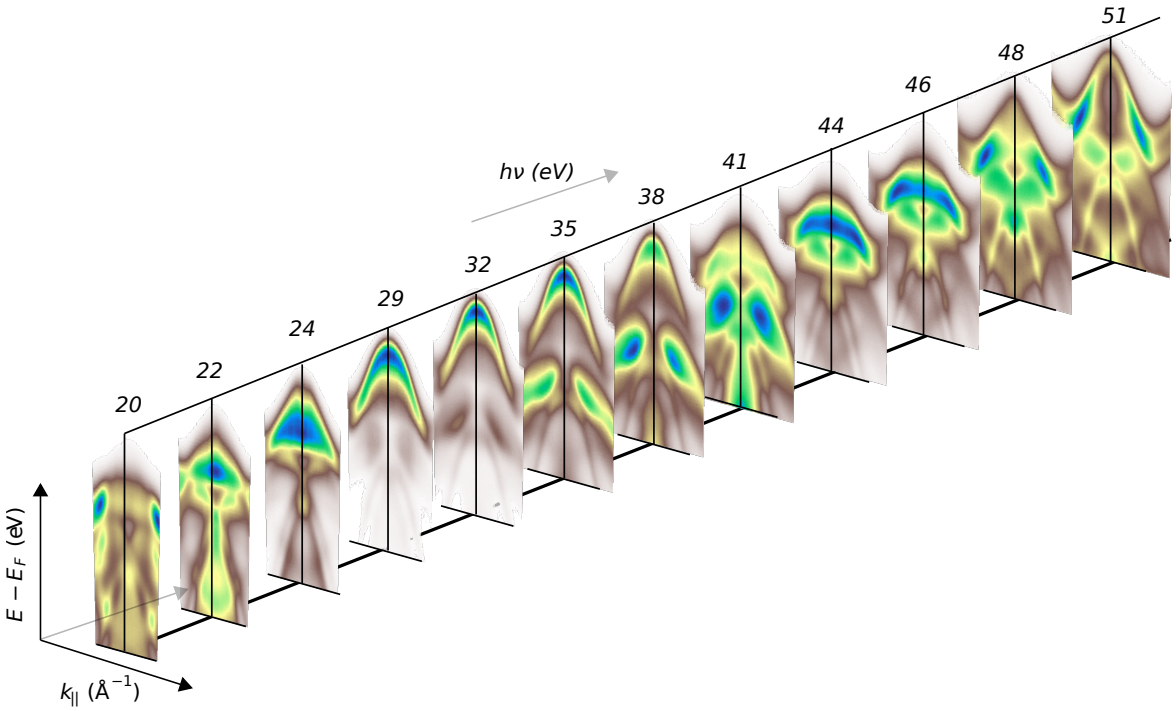

Figure 2: Series of ARPES-images recorded on the N-layer (N=6-7) WSe_2/Gr-SiC sample showing the dispersion along $k_{\|}$ for chosen photon energies between 20 and 90 eV. The vertical black line is at $k_{\|}$=0.

To have a clear view of the k_z-dispersion along $\Gamma - A$, we plot this cut at $k_{\|}$=0 as a function of the perpendicular component of the wave vector on Figure 3 for the different samples (same data as a function of the photon energy are available in the Supporting Information). Figures 3(b-d) show the raw data for 2, 3 and N-layers samples. For the 2-layer sample, the two bands which are the closest to the Fermi level clearly have a discontinuous k_z-dispersion. It consists in line segments corresponding to k_z-values where these bands appear at $k_{\|}$=0 in the $\Gamma - K$ dispersion. Hence, the top band is visible only for k_z between 3.1 and 3.5 Å^{-1} (photon energies between 23 and 40 eV); it then disappears to show up again between 4 and 4.6 Å^{-1} (50 and 70 eV). It has a low intensity from 4.5 to 5 Å^{-1} (70 to 80 eV) and becomes bright again from 5 Å^{-1} onwards (85 to 90 eV). It therefore appears and disappears when varying the photon energy, confirming the first observations made on Figure 1. Near, e.g., k_z = 3 or 3.7 Å^{-1} (20 eV and 43 eV) applying the rule 1 layer = one band at Γ, the sample is indistinguishable from a monolayer system with only one visible band at Γ. Let us note that this is the case around 21 eV, the photon energy produced by He-lamps. The same phenomenon is observable on the 3-layer sample with instead three bands appearing and disappearing. We note that the binding energies are slightly shifted in the 3-layer sample with respect to the 2-layer sample. This derives from the different thicknesses of the Gr-SiC substrate which induce differentiated charge transfers[16]. The reader can get more details in the Supporting Information. Nevertheless, the bright segments are shorter in photon energy and more numerous for each band. It starts to draw the clear band oscillations that we clearly see in the N-layer case, where the observed dispersion compares well with previously measured data on bulk-WSe_2[10,11]. The same observations can be made on the second derivative images (Figure 3(e-g)).

At these very small thicknesses, the electronic states considered here can certainly be seen as 2D-electronic systems, confined within the few atomic layers forming the WSe_2-layer. They can then be described as quantum well states whose behaviour in ARPES has been extensively described. The pioneering work of Louie *et al.*[17] was the first to evidence

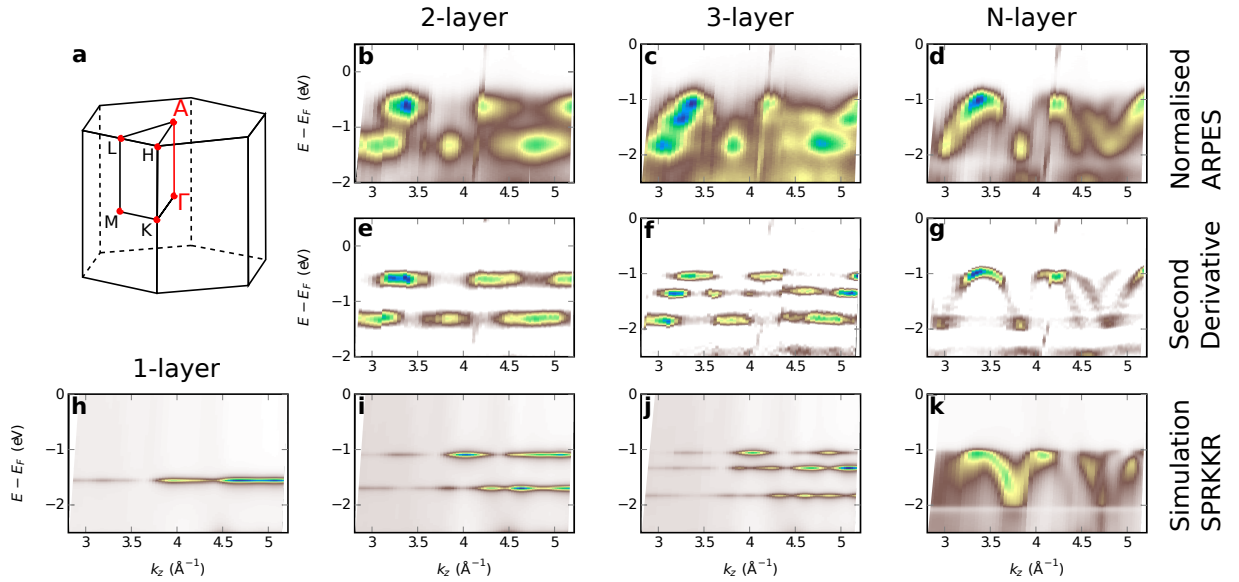

Figure 3: (a) First Brillouin zone of the WSe_2 reciprocal space. (b-g) Experimental band intensity variations at Γ along the $\Gamma - A$ direction of the reciprocal space for 2 (left), 3 (middle) and N (right) layers of WSe_2. Panels (b-d) show the raw data and panels (e-g) their second derivative. Panels (i-k) show the corresponding calculations done in the KKR-Green's function formalism (see text for details) with an additional calculation for 1-layer WSe_2 (h). The $h\nu$ to k_z conversion was done using $V_0 = 13$ eV for all spectra (See Supporting Information).

intensity variations of the Cu(111) Schockley surface state when varying the photon energy, with maxima for k_z-final states corresponding to the L-point of the 3D Brillouin zone. Intensity resonances of surface states using photon energies matching vertical transitions at high symmetry points of the 3D Brillouin zones was later confirmed by, e.g., studies on the Al(001)[18] or Cu-vicinal surfaces[19]. This is precisely what we observe here, although with some complications coming from the WSe_2 crystallographic structure. Taking a c-parameter of 12.96 Å[20], one obtains a $\Gamma - A$ distance of 0.2424 Å^{-1}. At low thicknesses (2 and 3-layer samples), the maxima observed in our data (around 3.15, 4.12 and 5.1 Å^{-1}) correspond to the positions of the A_6, A_8 and A_{10}-points of the reciprocal space. These maxima are observable on all the samples. The periodicity appears therefore as doubled in the reciprocal space, as compared to what is expected. This has been explained by Finteis *et al.*[9], following the works of Pescia *et al.*[21]. WSe_2 has a hexagonal structure whose primitive cell contains two WSe_2-layers (2H-WSe_2). It belongs to the D^4_{6h}-space group which is nonsymmorphic, *i.e.*, it

includes a screw axis which is located in the center of the unit cell along the c-axis. Group theory implies selection rules for photoemission from the Bloch states on the $\Gamma - A$ line of the Brillouin zone that are restricted to the subgroups of Δ_1 and Δ_2 symmetry, respectively, which together with the even parity required for coupling to a free-electron final state, results to allowed optical transition from a given initial state every other Brillouin zone[9].

Our results look very much alike what was obtained on graphene by Ohta *et al.*[22]. On a single layer sample, they showed that the π-orbital (forming the famous Dirac cone at the K-point of the reciprocal space) is confined in the crystal plane and show no k_z-dispersion. As the number of graphene layers increases, the number of π-orbital increases because of interlayer interactions and more and more discrete states appear, gradually converging towards the final 3D-dispersion[22]. This is clearly the model system to which our data on WSe_2 should be compared. An apparent doubling of the reciprocal space periodicity is also observed, since graphite structure also belongs to a nonsymmorphic space group[21]. The interpretation of these results was nicely revisited by Strocov in 2018[23]. In this work, ARPES is first interpreted in a Fourier-transform formalism and quantum confined 2D-states are introduced as standing waves multiplied by an envelope function quickly decreasing away from the surface. This lucid model not only confirms that intensity maxima should appear in ARPES at high symmetry points along k_z, but also predicts that these maxima spread over a k_z-range inversely proportional to the z-spatial extension of the 2D-state[23]. In other words, the "dots" observed at fixed binding energies should gradually shorten as the z-delocalization increases. This is what is observed on graphene[22] as well as in our results. Finally, let us note that this intensity behaviour is also well-reproduced by tight-binding calculations performed on a one-dimensional atomic chain of increasing length[24]. In the following, we'll show that different theoretical models can account for this behaviour, including fine details.

To understand better its physics, we propose to study the system at different levels of approximation using first a tight-binding initial state and free electron (FE) final state (TB-FE model). We then increase the complexity by describing the photoemission process

within the one-step model of photoemission[25] as implemented in the SPRKKR package[26] using a free electron final state (1-step-FE model). The last step is the calculation using the one-step model and a time-reversed LEED (TrLEED) final state (1-step-TrLEED model). This last result is presented in Figure 3(h-k) for free-standing 1, 2, 3 and an infinite number of WSe_2 layers. They are in excellent agreement with the measured data, reproducing the discontinuous patterns and converging to a bulk-like dispersion.

The tight-binding model[27] is inspired from the derivation made in references 11 and 28. We aim at a minimal model valid at Γ along the k_z direction. For more complete derivations, the reader can refer to references 28–32. More details about our tight-binding model and the calculation of the photoemission current can be found in the Supporting Information. Figure 4 shows the results of the three types of calculation on the trilayer system. In Figure 4(a), we see that the simple tight-binding model already captures the essential characteristics of the system with discrete energy states appearing in k_z-ranges in a staggered fashion. It underestimates the total amplitude of the dispersion (difference between the lowest level and highest energy level) of 0.2 eV (See Supporting Information for a quantitative comparison of these energy differences at Γ and K). The intensities are only indicative and the model does not resolve the complex symmetry effects due to the screw-axis[9]. For this reason, we only show the contribution of the phase corresponding to the dominant photoemission intensity in experiments ($\varphi = 2\pi/c$, $c/2$ being the interlayer distance, see Supporting Information). Figure 4(b) shows the results for the 1-step-FE model. They are strikingly similar to those of the TB-FE model. They nevertheless show a better agreement with experimental data: the values of the energy levels are more precisely calculated (with discrepancies smaller than 20 meV) and the photoemitted intensity displays additional modulation along k_z. The symmetry effects due to the crystal space group are now consistent with the experimental data. The pattern matches especially well with the measurements in the 2.5 to 4 $Å^{-1}$ k_z-range. Finally, Figure 4(c) shows the outcome of the 1-step-TrLEED model. In essence, the modulation of intensity is a step closer to experimental data. The k_z-patterning matches

extremely well the experiment in the 3.5 to 5.5 Å^{-1} range. On the other hand, we notice a discrepancy with an excess intensity in the 4.5 Å^{-1} and onwards range for the top band at -1 eV. Comparing ARPES dispersions in Figure 4(d,e), we see that the 1-step-FE model grossly overestimates the spectral weight of lower energy bands comparatively to those at the top of the valence bands. In the 1-step-TrLEED, the distribution of the spectral weight is improved: the top of the valence bands generally has a higher intensity than the lower lying bands in the experimental data (see Figure 4(f)).

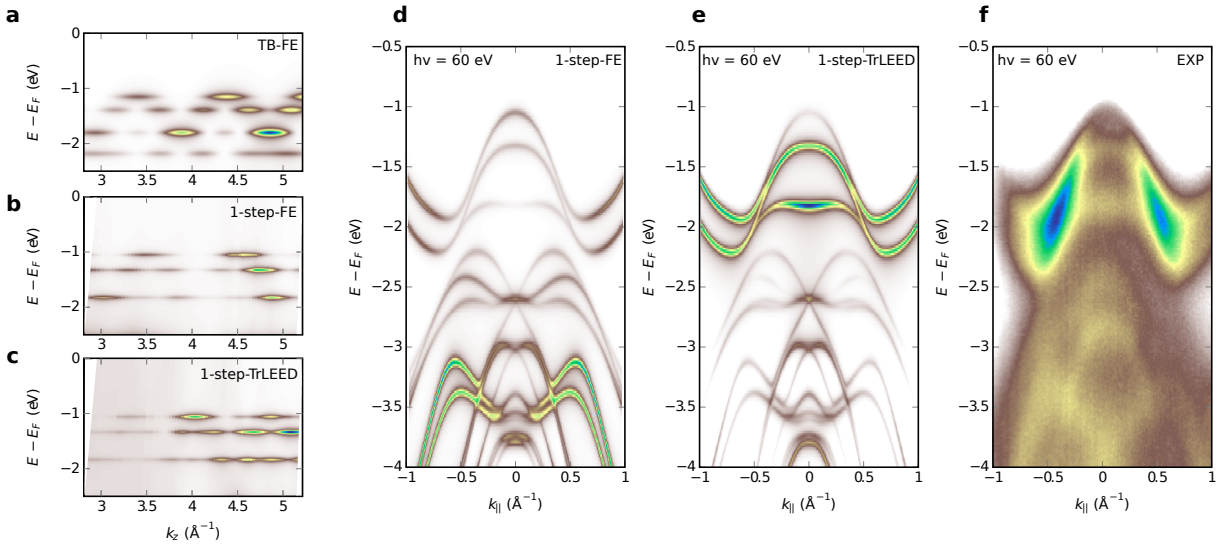

Figure 4: k_z-dispersions for the 3-layer system (a) from tight-binding initial state and free electron final state model (TB-FE), (b) from Bloch spectral function initial state and free electron final state (1-step-FE), (c) from Bloch spectral function initial state and time-reversed LEED final state (1-step-TrLEED). (c) is normalised to the background intensity. 3-layer sample ARPES dispersion at Γ for $h\nu = 60$ (d) calculated in the 1-step-FE model, (e) from the 1-step-TrLEED model and (f) as measured by ARPES. No normalization of intensities have been applied for (d-f).

To conclude, the ARPES study of MBE-deposited WSe_2 films with variable thickness gives an overview of the evolution of the electronic structure of this TMD during its transition from 2D to 3D. The behaviour observed at thicknesses as low as 2 or 3-layer WSe_2, with discrete states appearing at constant binding energies over finite k_z-ranges, are coherent with the predicted signature of 2D-states, confined in the plane of the atomically-thin crystal. Their evolution with an increasing number of layers shows a larger and larger delocalisation

as interlayer electronic hoppings become possible. A 6-7 layer film already shows an electronic structure comparable to what was measured on bulk crystals. Phenomenological[23] or simplified[24] models, as well as what is usually observed in 2D surface states account well for our observations, highly similar to what was previously measured on graphene layers[22]. Here, the results were completely modeled by various methods with increasing complexity, as a bench test for these models: a simple tight-binding model accounts for most of the experimental observations but does not capture the effects of the crystal symmetry on the photoemission signal. An *ab initio* calculation in the KKR-Green's function formalism using a free electron final state is more accurate but fails to reproduce the observed relative intensities of the different bands. A similar calculation using a TrLEED final state improves a lot this aspect. These last two calculations are performed on systems with the real geometry, going from 2D to 3D. The electronic properties of TMD, e.g., the nature (indirect or direct) of their band gap, strongly vary with thickness, both in "classical" TMD[33,34], or in more sophisticated but close compounds[8]. It is therefore of prime interest to know how the electronic structure evolves, as described by our results.

Associated content

Additional experimental details, materials, and methods

Acknowledgments

R.S. acknowledges the support of the French National Research Agency (ANR) (CORNFLAKE project, ANR-18-CE24-0015-01). This work was supported by the project Quantum materials for applications in sustainable technologies (QM4ST), funded as project No. CZ.02.01.01/00/22_008/0004572 by Programme Johannes Amos Commenius, call Excellent Research. This publication was supported by the project TWISTnSHINE, funded as project No. LL2314 by Programme ERC CZ.

References

(1) Novoselov, K. S.; Geim, A. K.; Morozov, S. V.; Jiang, D.; Zhang, Y.; Dubonos, S. V.; Grigorieva, I. V.; Firsov, A. A. Electric Field Effect in Atomically Thin Carbon Films. Science **2004**, 306, 666–669.

(2) Novoselov, K.; Jiang, D.; Schedin, F.; Booth, T.; Khotkevich, V.; Morozov, S.; Geim, A. Two-dimensional atomic crystals. Proceedings of the National Academy of Sciences **2005**, 102, 10451–10453.

(3) Dickinson, R. G.; Pauling, L. The crystal structure of molybdenite. J. Am. Chem. Soc. **1923**, 45, 1466–1471.

(4) Gatti, G. et al. Flat Γ Moiré Bands in Twisted Bilayer WS_2. Physical Review Letters **2023**, 131, 046401.

(5) Yuan, L.; Zheng, B.; Kunstmann, J.; Brumme, T.; Kuc, A. B.; Ma, C.; Deng, S.; Blach, D.; Pan, A.; Huang, L. Twist-angle-dependent interlayer exciton diffusion in WS_2–WSe_2 heterobilayers. Nature Materials **2020**, 1–7.

(6) Stansbury, C. H. et al. Visualizing electron localization of WS_2/WSe_2 moiré superlattices in momentum space. Science Advances **2021**, 7, eabf4387.

(7) Khalil, L.; Pierucci, D.; Velez-Fort, E.; Avila, J.; Vergnaud, C.; Dudin, P.; Oehler, F.; Chaste, J.; Jamet, M.; Lhuillier, E.; Pala, M.; Ouerghi, A. Hybridization and localized flat band in the $WSe_2/MoSe_2$ heterobilayer. Nanotechnology **2022**, 34, 045702.

(8) Ernandes, C.; Khalil, L.; Almabrouk, H.; Pierucci, D.; Zheng, B.; Avila, J.; Dudin, P.; Chaste, J.; Oehler, F.; Pala, M.; Bisti, F.; Brulé, T.; Lhuillier, E.; Pan, A.; Ouerghi, A. Indirect to direct band gap crossover in two-dimensional $WS_{2(1-x)}$ Se_{2x} alloys. npj 2D Materials and Applications **2021**, 5, 1–7.

(9) Finteis, T.; Hengsberger, M.; Straub, T.; Fauth, K.; Claessen, R.; Auer, P.; Steiner, P.; Hüfner, S.; Blaha, P.; Vögt, M.; Lux-Steiner, M.; Bucher, E. Occupied and unoccupied electronic band structure of WSe_2. Physical Review B **1997**, 55, 10400–10411.

(10) Riley, J. M. et al. Direct observation of spin-polarized bulk bands in an inversion-symmetric semiconductor. Nature Physics **2014**, 10, 835–839.

(11) Kim, B. S.; Rhim, J.-W.; Kim, B.; Kim, C.; Park, S. R. Determination of the band parameters of bulk 2H-MX_2 (M=Mo, W; X=S, Se) by angle-resolved photoemission spectroscopy. Scientific Reports **2016**, 6, 36389.

(12) Nguyen, P. V.; Teutsch, N. C.; Wilson, N. P.; Kahn, J.; Xia, X.; Graham, A. J.; Kandyba, V.; Giampietri, A.; Barinov, A.; Constantinescu, G. C.; Yeung, N.; Hine, N. D. M.; Xu, X.; Cobden, D. H.; Wilson, N. R. Visualizing electrostatic gating effects in two-dimensional heterostructures. Nature **2019**, 572, 220–223.

(13) Miwa, J. A.; Dendzik, M.; Grønborg, S. S.; Bianchi, M.; Lauritsen, J. V.; Hofmann, P.; Ulstrup, S. Van der Waals Epitaxy of Two-Dimensional MoS_2–Graphene Heterostructures in Ultrahigh Vacuum. ACS Nano **2015**, 9, 6502–6510.

(14) Salazar, R. et al. Visualizing Giant Ferroelectric Gating Effects in Large-Scale $WSe_2/BiFeO_3$ Heterostructures. Nano Lett. **2022**, 22, 9260–9267.

(15) Dau, M. T.; Vergnaud, C.; Gay, M.; Alvarez, C. J.; Marty, A.; Beigné, C.; Jalabert, D.; Jacquot, J.-F.; Renault, O.; Okuno, H.; Jamet, M. van der Waals epitaxy of Mn-doped $MoSe_2$ on mica. APL Materials **2019**, 7, 051111.

(16) Zhang, Y.; Xie, X.; Zong, J.; Chen, W.; Yu, F.; Tian, Q.; Meng, Q.; Wang, C.; Zhang, Y. Charge transfer between the epitaxial monolayer WSe_2 films and graphene substrates. Applied Physics Letters **2021**, 119, 111602.

(17) Louie, S. G.; Thiry, P.; Pinchaux, R.; Pétroff, Y.; Chandesris, D.; Lecante, J. Periodic Oscillations of the Frequency-Dependent Photoelectric Cross Sections of Surface States: Theory and Experiment. Phys. Rev. Lett. **1980**, 44, 549–553.

(18) Hofmann, P.; Søndergaard, C.; Agergaard, S.; Hoffmann, S. V.; Gayone, J. E.; Zampieri, G.; Lizzit, S.; Baraldi, A. Unexpected surface sensitivity at high energies in angle-resolved photoemission. Phys. Rev. B **2002**, 66, 245422.

(19) Lobo, J.; Mascaraque, A. Observation of the noble-metal L-gap surface state in Cu(311). Journal of Physics: Condensed Matter **2006**, 18, L395.

(20) Schutte, W.; De Boer, J.; Jellinek, F. Crystal structures of tungsten disulfide and diselenide. Journal of Solid State Chemistry **1987**, 70, 207–209.

(21) Pescia, D.; Law, A.; Johnson, M.; Hughes, H. Determination of observable conduction band symmetry in angle-resolved electron spectroscopies: Non-symmorphic space groups. Solid State Communications **1985**, 56, 809–812.

(22) Ohta, T.; Bostwick, A.; McChesney, J. L.; Seyller, T.; Horn, K.; Rotenberg, E. Interlayer Interaction and Electronic Screening in Multilayer Graphene Investigated with Angle-Resolved Photoemission Spectroscopy. Phys. Rev. Lett. **2007**, 98, 206802.

(23) Strocov, V. Photoemission response of 2D electron states. Journal of Electron Spectroscopy and Related Phenomena **2018**, 229, 100–107.

(24) Moser, S. An experimentalist's guide to the matrix element in angle resolved photoemission. Journal of Electron Spectroscopy and Related Phenomena **2017**, 214, 29–52.

(25) Braun, J.; Minár, J.; Ebert, H. Correlation, temperature and disorder: Recent developments in the one-step description of angle-resolved photoemission. Physics Reports **2018**, 740, 1–34, Correlation, temperature and disorder: Recent developments in the one-step description of angle-resolved photoemission.

(26) Ebert, H.; Ködderitzsch, D.; Minár, J. Calculating condensed matter properties using the KKR-Green's function method—recent developments and applications. Reports on Progress in Physics **2011**, 74, 096501.

(27) Salazar, R. Code available at `https://gitlab.com/SLZ_Raph/arpestb`, `https://gitlab.com/SLZ_Raph/arpestb`.

(28) Amorim, B. General theoretical description of angle-resolved photoemission spectroscopy of van der Waals structures. Physical Review B **2018**, 97, 165414.

(29) Cappelluti, E.; Roldán, R.; Silva-Guillén, J. A.; Ordejón, P.; Guinea, F. Tight-binding model and direct-gap/indirect-gap transition in single-layer and multilayer MoS_2. Physical Review B **2013**, 88, 075409.

(30) Roldán, R.; López-Sancho, M. P.; Guinea, F.; Cappelluti, E.; Silva-Guillén, J. A.; Ordejón, P. Momentum dependence of spin–orbit interaction effects in single-layer and multi-layer transition metal dichalcogenides. 2D Materials **2014**, 1, 034003.

(31) Fang, S.; Kuate Defo, R.; Shirodkar, S. N.; Lieu, S.; Tritsaris, G. A.; Kaxiras, E. Ab initio tight-binding Hamiltonian for transition metal dichalcogenides. Physical Review B **2015**, 92, 205108.

(32) Silva-Guillen, J. A.; San-Jose, P.; Roldan, R. Electronic Band Structure of Transition Metal Dichalcogenides from Ab Initio and Slater–Koster Tight-Binding Model. Applied Sciences **2016**, 6, 284.

(33) Mak, K. F.; Lee, C.; Hone, J.; Shan, J.; Heinz, T. F. Atomically Thin MoS_2: A New Direct-Gap Semiconductor. Phys. Rev. Lett. **2010**, 105, 136805.

(34) Radisavljevic, B.; Radenovic, A.; Brivio, J.; Giacometti, V.; Kis, A. Single-layer MoS_2 transistors. Nature Nanotechnology **2011**, 6, 147–150.